Analysis of Constructive Modifications for Enhancing the Performance of Solar Collector/Regenerators for Liquid Desiccant Systems

Fernando Manuel Gómez Castro[1], Ursula Eicker[2], Ulrike Jordan[1]

[1] Institute for Thermal Engineering, Kassel University, Kassel (Germany)

[2] Next-Generation Cities Institute, Concordia University Montreal, Montreal (Canada)

Abstract

This paper presents an investigation of a solar collector/regenerator (C/R) that is designed as a direct solar thermally-driven liquid desiccant system, in which the diluted desiccant solution is regenerated by simultaneously exposing it to solar radiation and air streaming along the liquid surface. Numerical finite element models of the device are developed to improve the heat and mass transfer processes within the collector/regenerator. Constructive modifications of the analysed design are based on adding an upper air-preheating channel, an artificially roughened absorber plate and a flat bottom reflector. The results demonstrate that the air-preheating channel has a moderate impact on the regeneration efficiency, whereas the turbulators and the solar concentrator exhibit high potential to boost the performance of the collector/regenerator.

Keywords: Thermally-driven liquid sorption system, collector/regenerator, numerical finite element models, upper air-preheating channel, turbulators, flat bottom reflector

1. Introduction

Solar-driven liquid desiccant systems are regarded as a sustainable and environmentally friendly technology to provide suitable thermal comfort conditions in buildings and to sanitise indoor air. The systems rely on the capacity of hygroscopic solutions to directly remove the moisture from the air by the absorption process and on the solar heat to regenerate the liquid sorbent within a temperature range of 40 to 80 °C (Katejanekarn and Kumar, 2008).

In a collector/regenerator (C/R), the heat collecting fluid is a hygroscopic liquid film flowing down the absorber plate. The liquid desiccant is reconcentrated by exposing it to air circulating in the regenerating channel. However, this device is not yet commercially available due to its large dimensions to satisfy the regeneration requirements of liquid desiccants. Large dimensions limit not only the wettability of the absorber plate but also its modularity and scalability, thus making it quite difficult to install it on the building envelope.

Some performance enhancement methods such as the double-glazed arrangement have been analysed in the literature for shortening the solar C/R length without damaging its operation. By using the counter-flow pattern between the liquid and gas phases, a performance improvement of about 3% was obtained for the device with upper air-preheating channel (Yang and Wang, 1998) under the hot and humid climatic conditions of Kaohsiung, Taiwan.

Zheng and Worek (1996) experimentally investigated a mechanical method for enhancing the heat and mass transfer during the evaporation of water from a liquid film in a channel consisting of adding cylindrical rods to a plate transversely to the direction of fluid motion. The average Nusselt and Sherwood numbers first increased to peak values at an optimal spacing of the rods and then decreased with further augmentation in rod pitch since the eventual diminution in surface roughness reduced both the flow separation/reattachment processes in the gas-phase and the mixing in the liquid-phase.

Flat reflectors are a well-established, cost-effective way to boost the operation of solar devices. Chen and Kao (1990) experimentally compared the performances of a closed C/R, a natural-flow C/R and a natural-flow C/R augmented with an external flat reflector using LiCl solution with mass fractions between 30% and 35%. The results demonstrated that adding a reflective mirror enhanced the evaporation rate by 20%.

Selection and/or peer review under responsibility of Scientific Committee
doi:10.18086/eurosun.2022.06.05 Available at http://proceedings.ises.org

This paper presents a numerical investigation of constructive modifications for promoting the heat and mass transfer phenomena in the regenerating panel. The modifications include the attachment of an upper air-preheating channel. In a second step, an artificially roughened absorber plate is used. Furthermore, a ray tracing algorithm is developed in Mathematica to evaluate the contribution of a flat bottom mirror to the optical performance of a south-facing C/R under the typical meteorological conditions of Stuttgart, Germany.

2. Heat and mass transfer in solar collector/regenerators

Fig. 1 shows the investigated C/R constructions. The upper air-heating channel shown in Fig. 1(a) is constructed with an additional glass cover on top of the existing one with a change in flow direction of the air at the end of the device. The roughened absorber plate shown in Fig. 1(b) is modelled as multiple V dimpled patterns from computational models implemented in Wolfram Mathematica. To evaluate the impact shading between the C/R and the flat bottom mirror a construction as shown in Fig. 1(c) is considered.

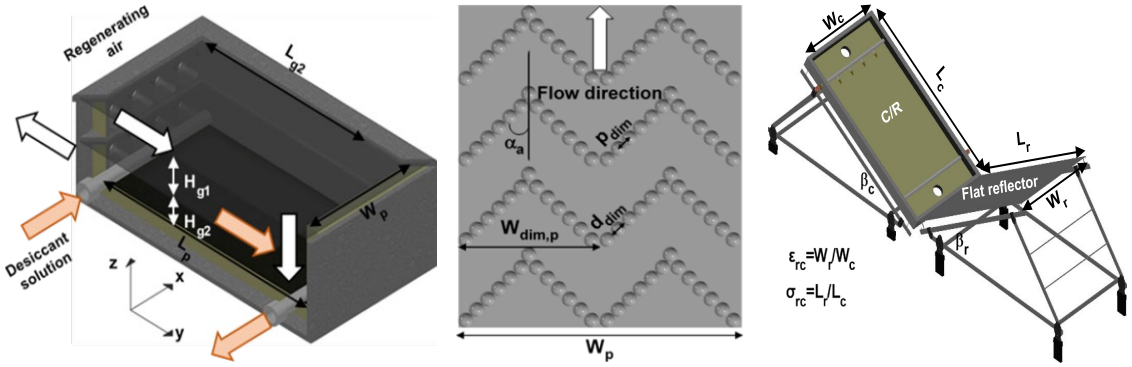

(a) Upper air-preheating channel (double-pass double-glazed C/R)

(b) Artificially roughened absorber plate (dimples)

(c) Flat bottom reflector

Fig. 1: Analysed constructive modifications of the solar collector/regenerator.

2.1. Single-pass single-glazed collector/regenerator

Six nodes normal to the flow directions of the fluids are used to analyse the coupled heat and mass fluxes in the finite element of the single-pass single-glazed C/R (SG-C/R) as shown in Fig. 2. These are: (I) the glass cover, (II) regenerating air, (III) desiccant solution, (IV) porous fabric, (V) absorber plate and (VI) collector housing.

To model the heat and mass transfer, a basic set of equations was developed based on the mass and energy balances for each node.

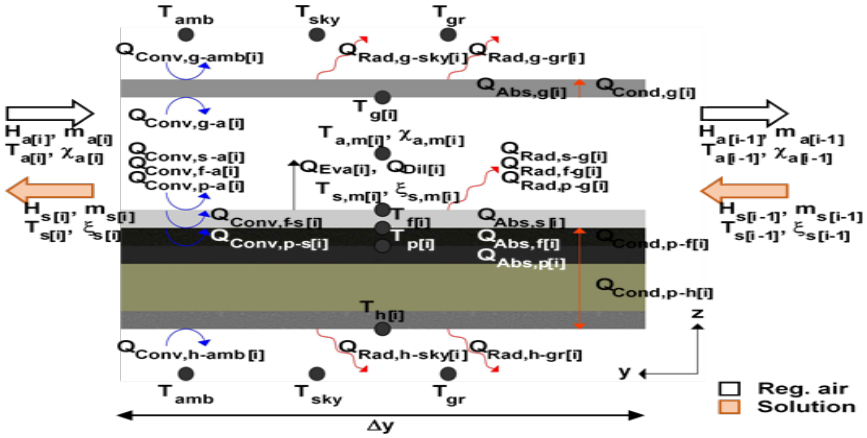

Fig. 2: Finite element of the single-pass single-glazed C/R in counter-flow.

2.2. Double-pass double-glazed collector/regenerator

The finite element of the double-pass double-glazed C/R (DG-C/R) illustrated in Fig. 3 comprises eight nodes normal to the flow directions of the fluids. These are: (I) the outer glass cover, (II) regenerating air in upper channel, (III) inner glass cover, (IV) regenerating air in lower channel, (V) desiccant solution, (VI) porous fabric,

(VII) absorber plate and (VIII) collector housing.

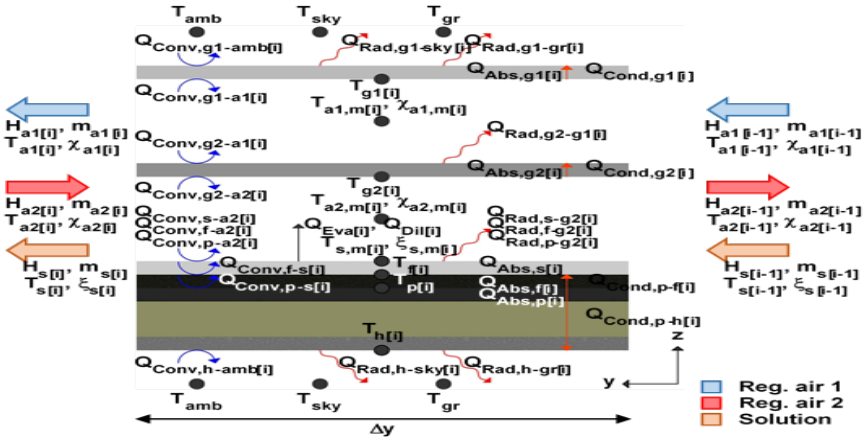

Fig. 3: Finite element of the double-pass double-glazed C/R in counter-flow.

The DG-C/R model is an extension of the SG-C/R model with an additional upper channel with transparent walls for preheating the air stream prior to the solution regeneration process. Therefore, the set of governing equations from the SG-C/R is extended by three additional ones describing the energy balance of the outer glass cover, of the regenerating air in the upper channel, and the inner glass cover.

The combined effects of the thermal and solutal buoyancy forces on the mixed convective heat and mass transfer during water evaporation from the liquid desiccant film in a smooth channel are considered by applying the law of cosines to the correlations proposed by Azevedo and Sparrow (1985) (natural convection) and by Gnielinski (2010) (forced convection) for laminar air flow and to those given by Fedorov and Viskanta (1997) (natural convection) and by Taler (2017) (forced convection) for turbulent air flow. In the case of an artificially roughened channel, the calculations for the forced flow are done based on the unified formulation developed by Brkic and Praks (2018), in which the correlations of Kumar et al. (2017) for multiple V-dimpled patterns are used in the fully developed rough turbulent regime.

2.3. Solar concentration with a flat bottom reflector

The optical path of a sunlight ray through the concentrating system can be fully described from the vector analysis based on transformation matrices among the coordinate systems of the horizontal (X, Y, Z), reflector (X', Y', Z') and collector (X'', Y'', Z'') planes. Fig. 4 shows the shading of the flat reflector by the collector, which can occur if the sun is situated behind the receiver. This situation leads not only to the self-shading of the collector but also to the total/partial obstruction of the sunlight falling on the opposite bottom mirror.

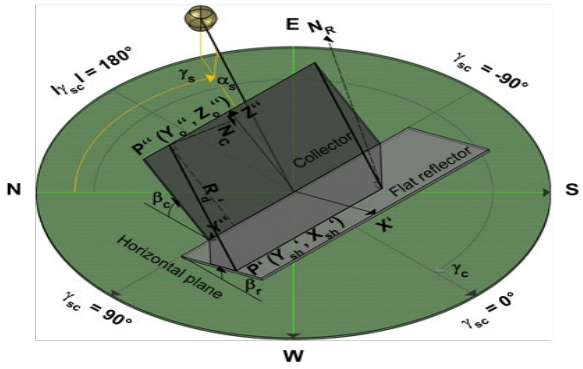

Fig. 4: Intersection point (Ysh', Xsh') of a sunlight ray transmitted from the collector to the reflector.

Fig. 5(a) shows the self-shading of the reflective surface, which simultaneously casts a total or partial shadow on the opposite collector. The optical path of the sunlight rays incident on and reflected by the flat booster mirror towards the collector plane is depicted in Fig. 5(b). Some of these rays are accepted on the receiver aperture area, while others are lost.

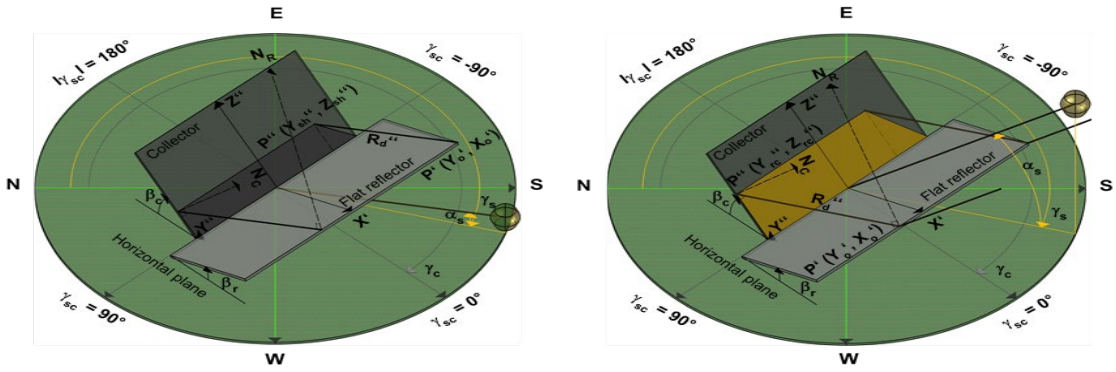

(a) (b)

Fig. 5: Intersection points of a sunlight ray (a) transmitted from the reflector to the collector and (b) reflected from the reflector to the collector.

Convex 2D polygons that describe the shading onto the collector and reflector planes as well as the sunlight concentrated by the mirror onto the collector plane are clipped in turn against each boundary of these surfaces according to the algorithm of Sutherland-Hodgman (1974) to estimate the available global irradiance on the tilted receiver from the method of Baccoli et al. (2018).

3. Performance indicators

In order to characterise the mass transfer mechanism of the studied devices, the regeneration efficiency (η_{Des}) is introduced as the ratio of the latent heat required by the desorption of the water from the diluted desiccant solution trickling down the absorber plate (ΔH_{Des}) to the global irradiance on the aperture area of the tilted collector ($Q_{\beta c}$) (Peng and Zhang, 2015):

$$\eta_{Des}=\frac{\Delta H_{Des}}{\dot{Q}_{\beta c}}\times 100=\frac{\dot{m}_{Des}\cdot\left(h_{fg}+h_{Dil}\right)}{G_{\beta c}\cdot A_c}\times 100 \qquad \text{(eq. 1)}$$

With $\dot{m}_{Des}$ as the water desorption rate; h_{fg} as the enthalpy of evaporation; h_{Dil} as the specific enthalpy of dilution; $G_{\beta c}$ as the global solar irradiance collected on the tilted surface; A_c as the aperture area of the collector.

For the purpose of considering the power required to blow air through an artificially roughened channel, the thermohydraulic performance factor ($PF_{th,SGr}$) is assessed (Lewis, 1975):

$$PF_{th,SGr}=\frac{Nu_{Dh,SGr}/Nu_{Dh,SG}}{\left(f_{d,SGr}/f_{d,SG}\right)^{1/3}} \qquad \text{(eq. 2)}$$

Where $Nu_{Dh,SGr}$ and $f_{d,SGr}$ are the Nusselt number and Darcy friction factor for the structured duct, whereas $Nu_{Dh,SG}$ and $f_{d,SG}$ are the Nusselt number and Darcy friction factor for the smooth channel.

Additionally, the optical performance factor (PF_{opt}) denotes the potential benefit/drawback of coupling a flat bottom reflector to the collector/regenerator. It is defined as the ratio of the global tilted solar radiation harvested by the boosted regeneration unit ($I_{\beta rc}$) to the global tilted solar radiation collected by the conventional one without reflecting surface ($I_{\beta c}$) during a given time period (Rehman and Uzair, 2021):

$$PF_{opt}=\frac{I_{\beta rc}}{I_{\beta c}}=\frac{\int G_{\beta rc}\cdot dt}{\int G_{\beta c}\cdot dt} \qquad \text{(eq. 3)}$$

With $G_{\beta rc}$ and $G_{\beta c}$ as the global solar irradiance on the tilted receiver with and without the booster mirror.

4. Results and discussion

4.1. Double-pass double-glazed collector/regenerator

The single-pass single-glazed (SG-C/R) and double-pass double-glazed collector/regenerators (DG-C/R) with smooth absorber plates are compared for the same operating conditions with aqueous LiCl as desiccant solution. The parameters taken into account along with their values are listed in Tab 1.

Tab. 1: Ranges and reference values of the control parameters for SG- and DG-C/Rs.

Type	Variable	Symbol	Unit	Range	Reference value
Meteorological parameters	Global solar irradiance on the tilted surface	$G_{\beta c}$	W/m^2	400, 700, 1000	700
	Barometric pressure	p_b	Pa	-	97657
	Wind speed	V_w	m/s	-	2
Parameters of the air	Inlet temperature	$T_{a,in}$	°C	-	30
	Inlet humidity ratio	$\chi_{a,in}$	g/kg	-	12
	Volumetric flow rate per cross-sectional area	$\dot{V}_a$	$m^3/(m^2 \cdot h)$	200-3600	-
Parameters of the desiccant solution	Inlet temperature	$T_{s,in}$	°C	-	40
	Inlet mass fraction	$\xi_{s,in}$	%	-	30
	Volumetric flow rate per cross-sectional area	$\dot{V}_s$	$l/(m^2 \cdot h)$	-	500
Geometric parameters	Width × length	$W_c \times L_c$	m × m	-	1 × 2
	Gap height(s)	H_{gi}	cm	-	5
	Tilt angle	β_c	°	-	35°

The ratio of the regeneration efficiency of the double-pass double-glazed C/R to that of the single-pass single-glazed one is plotted for Reynolds numbers of the air (with the channel hydraulic diameter D_h as characteristic length) of $Re_{a,Dh} \in [314, 6033]$ and a Reynolds number of the liquid desiccant of $Re_s^*=12.8$, see Fig. 6(a). The three lines depict the efficiency ratios for an irradiance on the tilted collector surface of 400 W/m², 700 W/m² and 1000 W/m².

According to the left y-axis in Fig. 6(a), the efficiency ratio sharply decreases by increasing the air Reynolds number, which indicates that the second glass cover is only advantageous for low air Reynolds numbers. This happens since the temperature rise of the air passing the upper channel is also high for low air Reynolds numbers as shown in Fig. 6(b). The air-preheating is promoted at high irradiance levels, as the warmer liquid film transfers more heat to the inner glazing.

For irradiance levels of 400 W/m² and 1000 W/m², the DG-C/R outperforms the SG-C/R ($\eta_{Des,DG}/\eta_{Des,SG}>1$) in the laminar air flow regime with air Reynolds numbers below about 2100 and 1400, respectively (see left y-axis in Fig. 6(a)). That means, the higher the solar irradiance, the lower the maximum air Reynolds number with a positive effect of the air-preheating upper channel. This occurs because the greater solar heating of the desiccant solution at high irradiance levels requires greater air-preheating to reduce the thermal dissipation from the liquid film, which in turn enhances the mass transfer driving potential at the liquid-air interface.

From the right y-axis in Fig. 6(a), an upward trend in the regeneration efficiency is observed with augmenting air Reynolds number. In transitional and turbulent flow regimes, the additional glazing and air passage of the DG-C/R negatively affect the system performance. For a Reynolds number of the air of about 6000, corresponding to a mean air velocity in the channel of about 1 m/s and a solar irradiance on the tilted collector plane of 700 W/m², the regeneration efficiency of the DG-C/R drops by approximately 5.1% with respect to the SG-C/R, from $\eta_{Des,SG}=37.9\%$ to $\eta_{Des,DG}=36\%$. This occurs because the weak air-preheating prevailing in such conditions (see Fig. 6(b)) cannot sufficiently diminish the heat fluxes from the liquid desiccant to compensate for the low optical efficiency of the device. Thus, the highest performance benefit of the DG-C/R is obtained at low air flow rates under reduced sunlight conditions.

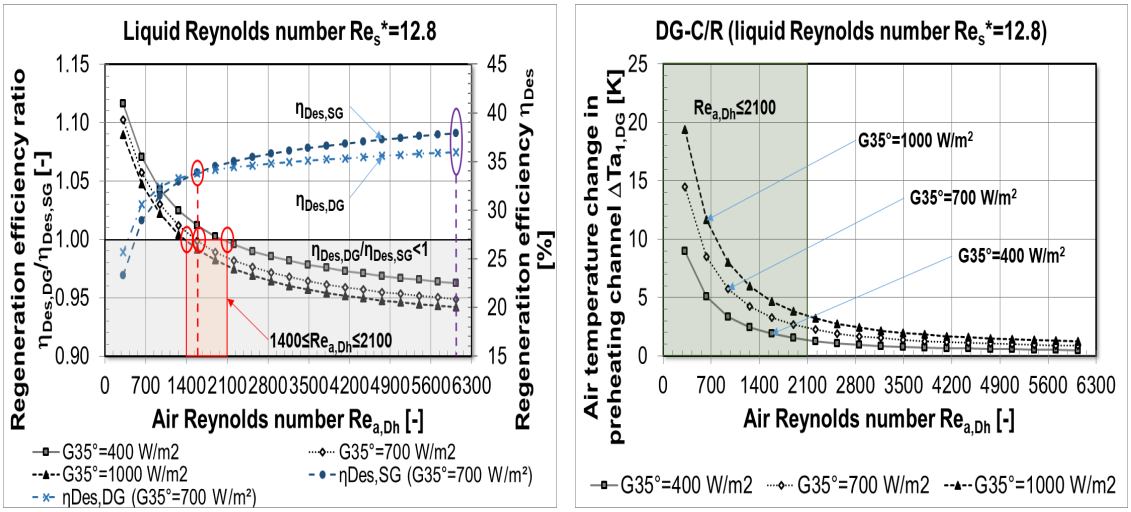

(a) Efficiency ratio

(b) Air-preheating effect

Fig. 6: Ratio of the regeneration efficiency of the DG-C/R with respect to the SG-C/R (a) and air-preheating effect (b) over the Reynolds number of the air at different global tilted solar irradiance levels.

4.2. Artificially roughened single-pass single-glazed collector/regenerator

The single-pass single-glazed collector/regenerators with smooth (SG-C/R) and artificially roughened (SGr-C/R) channels are benchmarked at the operating conditions and geometric parameters specified in Tab. 1 using aqueous LiCl as hygroscopic liquid. The absorber plate of the SGr-C/R is texturized by multiple V-dimples arranged according to the optimal configuration reported by Kumar et al. (2017) (see Fig. 1(b)) with a relative roughness depth of κ_r=0.037 (ratio of the dimple depth to the hydraulic diameter of the channel), relative roughness width of ω_r=5 (ratio of the plate width to the width of the dimpled pattern), δ_r=1 (ratio of the dimple depth to dimple diameter), relative roughness pitch of π_r=9 (ratio of the distance between two consecutive dimples to the dimple depth) and angle of attack of α_a=55° (angle between the dimple line and the air flow direction).

The left y-axis in Fig. 7(a) represents the ratio of the regeneration efficiency of the artificially roughened single-pass single-glazed C/R to that of the smooth single-pass single-glazed one for air Reynolds numbers ranging from 314 to 6033 and a liquid Reynolds number equal to 12.8. The efficiency ratio curves are obtained for solar irradiances on the tilted collector surface of 400 W/m², 700 W/m² and 1000 W/m². It is found that the SGr-C/R strongly outperforms the SG-C/R ($\eta_{Des,SGr}/\eta_{Des,SG}>1$) within the considered range of $Re_{a,Dh}$. This behaviour is even more noticeable at low solar irradiance thanks to the minor thermal dissipation of the liquid film with its surroundings.

According to the left y-axis in Fig. 7(a), the efficiency ratio first increases until it reaches its maximum value, after which it decreases smoothly with rising air Reynolds number. This fact reveals that there is a limit at which the remarkable intensifications in the convective heat and mass transfer coefficients caused by the successive flow separation/reattachment in the gas-phase and mixing in the liquid-phase can no longer compensate for the lessenings in the temperature and vapour pressure gradients at the liquid-air interface as the air flow rate augments. For irradiance levels of 400 W/m² and 1000 W/m², the optimal air Reynolds numbers lie in the early stage of the turbulent flow and in the transitional flow with $Re_{a,Dh}\approx4400$ and $Re_{a,Dh}\approx3800$, respectively. Thereby, the higher the solar irradiance, the lower the optimal air Reynolds number with the maximised operational benefit of the structured absorber plate. This can be explained by the fact that a lower convective heat transfer coefficient inhibits the thermal losses from the hotter liquid film at high solar irradiance collected on the tilted surface, which improves the mass transfer driving force.

The right y-axis in Fig. 7(a) shows an ascending tendency in the regeneration efficiency by increasing air Reynolds number. For $Re_{a,Dh}\approx6000$, corresponding to a mean air velocity in the channel of approximately 1 m/s, and a solar irradiance on the tilted collector surface of 700 W/m², the regeneration efficiency of the SGr-C/R rises by about 9.9% with respect to the SG-C/R, from $\eta_{Des,SG}$=37.9% to $\eta_{Des,SGr}$=41.7%, due to the combined effects of enhancing the convective heat and mass transfer coefficients by adding multiple V-dimples.

The thermohydraulic performance factor of the artificially roughened single-pass single-glazed C/R to that of the

smooth single-pass single-glazed one is plotted for air Reynolds numbers of $Re_{a,Dh} \in [314, 6033]$, a liquid Reynolds number of $Re_s^*=12.8$ and solar irradiances of 400 W/m², 700 W/m² and 1000 W/m² falling on the tilted absorbing surface, see Fig. 7(b). Values of $PF_{th,SGr}$ greater than unity denote the overall advantage of roughening the absorber plate of the SGr-C/R, since the most efficient device maximises the Nusselt number while minimising the friction factor and, consequently, the fan power consumption. The use of the SGr-C/R over the SG-C/R is recommended only for air Reynolds numbers beyond about 2500 with the thermohydraulic performance factor rising monotonically up to about 1.6.

The optimal operating points found for the SGr-C/R at $Re_{a,Dh}\approx4400$ and $Re_{a,Dh}\approx3800$ under solar irradiances of 400 W/m² and 1000 W/m² have thermohydraulic performance factors of $PF_{th,SGr}\approx1.3$ and $PF_{th,SGr}\approx1.1$, respectively, while the operating point $Re_{a,Dh}\approx6000$ at a solar irradiance of 700 W/m² reaches a value of $PF_{th,SGr}\approx1.5$. This demonstrates that the procedure for optimising the geometry and operating conditions of the SGr-C/R must be based on the combined analysis of the curves of efficiency ratio (see the left y-axis in Fig. 7(a)) and thermohydraulic performance factor (see Fig. 7(b)). By contrast, below $Re_{a,Dh}\approx2500$, modest increases in heat transfer are obtained within the structured channel in comparison to the high air flow pressure drops, so that the high energy requirements of the fan are not justified.

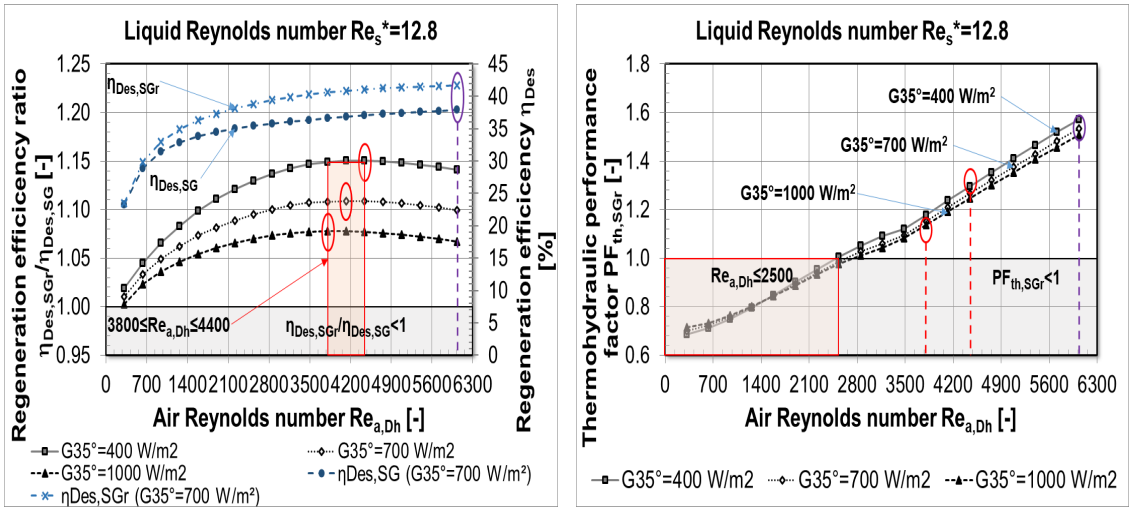

(a) Efficiency ratio

(b) Thermohydraulic performance factor

Fig. 7: Ratio of the regeneration efficiency (a) and thermohydraulic performance factor (b) over the Reynolds number of the air at different global tilted solar irradiance levels.

4.3. Solar collector/regenerator with booster mirror

Fig. 8. shows the contour plots of the total annual global radiation on the tilted surface ($I_{\beta rc}$) and the annual optical performance factor (PF_{opt}) for Stuttgart, Germany (48.8° N 9.2° E) obtained from the weather data of the typical meteorological year (TMY) generated by Meteonorm. The analysed low concentrating system comprises a C/R of 1 m width × 2 m length coupled to a flat bottom mirror with the same dimensions ($L_r/L_c=1$ and $W_r/W_c=1$) and a reflectivity of 0.9. The performance indicators $I_{\beta rc}$ and PF_{opt} are calculated for representative average days for each month throughout the year (Klein, 1977) with 5° steps for the inclinations of the collector ($0°\leq\beta_c\leq90°$) and reflector ($0°\leq\beta_r\leq90°$) by only discarding the case of $\beta_c=\beta_r=90°$. The total annual global solar radiation available on the C/R reaches a maximum value of about 1400 kWh/(m²Y) at collector inclinations of $30°\leq\beta_c\leq60°$ and reflector tilt angles of $10°\leq\beta_r\leq35°$ with annual optical performance factors of $1.05\leq PF_{opt}\leq1.12$. Finally, optical performance factors less than unity occur in the regions limited by $0°\leq\beta_c\leq90°$ and $40°\leq\beta_r\leq90°$, which indicates the shading of the collector either by itself (see Fig. 4) or by the planar mirror (see Fig. 5(a)).

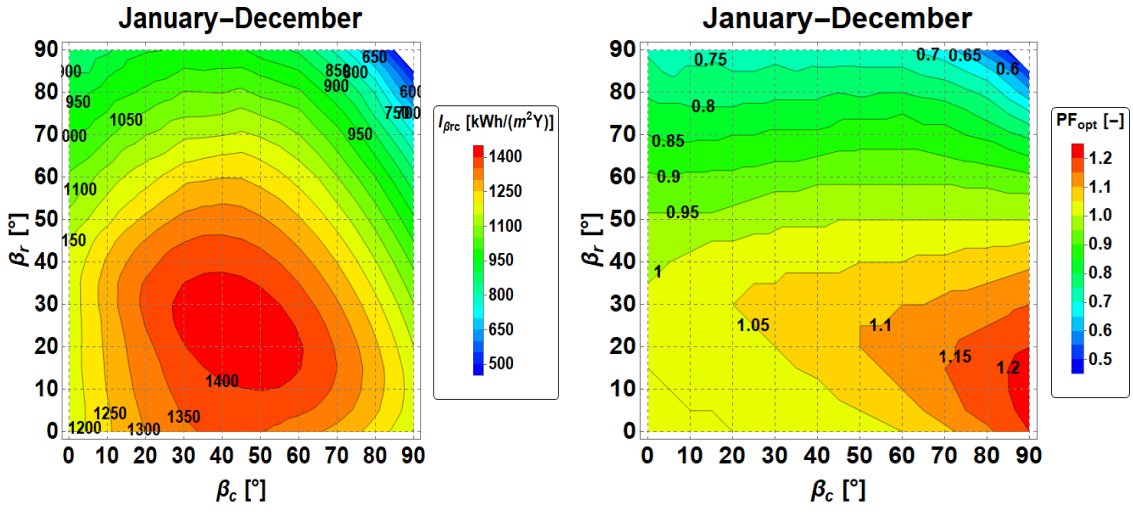

(a) (b)

Fig. 8: Variation of (a) the total annual global solar radiation on the tilted surface and (b) the annual optical performance factor for the C/R with booster reflector (L_r/L_c=1 and W_r/W_c=1) in Stuttgart, Germany.

5. Conclusions

This paper presents an investigation of the impact of three measures on the performance of a solar collector/regenerator: Adding an upper air-preheating channel, using a structured absorber plate and coupling a flat bottom mirror to the direct solar regeneration unit.

For the operating conditions and geometry considered here, it was found that the double-pass double-glazed configuration (DG-C/R) improves the regeneration efficiency relative to the single-pass single-glazed one (SG-C/R) for small Reynolds numbers. The reason for this lies in the fact that the air preheated in the double-pass construction contributes to decrease the thermal dissipation from the desiccant solution, which leads to an increase in the liquid-air interfacial vapour pressure gradient. However, this air preheating effect weakens as the air flow approaches the transitional and turbulent regimes and may even negatively impact the solution regeneration process. For example, for an air Reynolds number of approximately 6000, corresponding to a mean air velocity in the channel of about 1 m/s and a solar irradiance collected on the tilted plane of 700 W/m², the regeneration efficiency of the DG-C/R falls by about 5.1% with respect to the SG-C/R, from $\eta_{Des,SG}$=37.9% to $\eta_{Des,DG}$=36%.

In contrast, the structured single-pass single-glazed device (SGr-C/R) enhances the regeneration efficiency relative to the smooth single-pass single-glazed one (SG-C/R) by intensifying the convective heat and mass transfer coefficients via the continuous flow separation/reattachment in the gas-phase and mixing in the liquid-phase. The optimal values of air Reynolds numbers that maximise the efficiency ratios obtained for the analysed operating conditions and geometric configuration reveal the counterproductive effects of this measure on the temperature and vapour pressure gradients at the liquid-air interface (and consequently, on the effective mass flux of water vapour) if the device operates beyond them. For a Reynolds number of about 6000 and a solar irradiance available on the tilted collector of 700 W/m², the structured surface results in an increase of the regeneration efficiency by approximately 9.9%, from $\eta_{Des,SG}$=37.9% to $\eta_{Des,SGr}$=41.7%, and a thermohydraulic performance factor of 1.5.

Finally, a ray-tracing model was developed to evaluate the effect of an additional mirror on the collector efficiency. For a low concentrating system installed in Stuttgart, Germany, the maximum total annual global solar radiation yields to about 1400 kWh/(m²Y), which can be attained at collector tilt angles between 30° and 60° and reflector inclinations between 10° and 35°. This corresponds with an increase of the annual optical performance of 5 to 12%.

In order to realistically evaluate the suitability of the measures discussed here, annual simulations of the systems are necessary. Besides the heat and mass transfer exchanges occurring in the direct solar regenerators and the optical performance of the flat booster mirror described in the proposed models, other factors must be considered in the analyses such as the additional power consumption of the fan due to the upper channel and the 180° air

deflection in the DG-C/R and the structured absorber plate in the SGr-C/R as well as their construction and operating costs. This paper provides a good basis for this future research.

Acknowledgments

The funding provided by the Federal Ministry of Education and Research in framework of the program “Research at Universities of Applied Sciences-Funding Scheme Young Engineers” (contract number 03FH0041X4) during the initial stages of this research (2015-2018) is gratefully acknowledged.

References

Azevedo, L. F. A., Sparrow, E. M., 1985. Natural convection in open-ended inclined channels. Journal of Heat Transfer, 107(4), 893-901, DOI: 10.1115/1.3247518.

Baccoli, R., Frattolillo, A., Mastino, C., Curreli, S., Ghiani, E., 2018. A comprehensive optimization model for flat solar collector coupled with a flat booster bottom reflector based on an exact finite length simulation model. Energy Conversion and Management, 164, 482-507, DOI: 10.1016/j.enconman.2018.02.091.

Brkic, D., Praks, P., 2018. Unified friction formulation from laminar to fully rough turbulent flow. Applied Sciences, 8(11), 2036, DOI: 10.3390/app8112036.

Chen, L. C., Kao, F. K., 1990. The experimental study of three types of regenerator/collector for solar liquid desiccant cooling. Clean and Safe Energy Forever. International Solar Energy Society Proceedings Series, 1, 840-844, DOI: 10.1016/B978-0-08-037193-1.50171-3.

Fedorov, A. G., Viskanta, R., 1997. Turbulent natural convection heat transfer in an asymmetrically heated, vertical parallel-plate channel. International Journal of Heat and Mass Transfer, 40(16), 3849-3860, DOI: 10.1016/S0017-9310(97)00043-4.

Gnielinski, V., 2010. G2 Heat transfer in concentric annular and parallel plate ducts, in VDI Heat Atlas (2nd). Springer, Berlin, Heidelberg, pp. 701-708, DOI: 10.1007/978-3-540-77877-6_35.

Katejanekarn, T., Kumar, S., 2008. Performance of a solar-regenerated liquid desiccant ventilation pre-conditioning system. Energy and Buildings, 40(7), 1252-1267, DOI: 10.1016/j.enbuild.2007.11.005.

Klein, S. A., 1977. Calculation of monthly average insolation on tilted surfaces. Solar Energy, 19(4), 325-329, DOI: 10.1016/0038-092X(77)90001-9.

Kumar, A., Kumar, R., Maithani, R., Chauhan, R., Sethi, M., Kumari, A., Kumar, S., Kumar, S., 2017. Correlation development for Nusselt number and friction factor of a multiple type V-pattern dimpled obstacles solar air passage. Renewable Energy, 109, 461-479, DOI: 10.1016/j.renene.2017.03.030.

Lewis, M. J., 1975. Optimising the thermohydraulic performance of rough surfaces. International Journal of Heat and Mass Transfer, 18(11), 1243-1248, DOI: 10.1016/0017-9310(75)90232-X.

Peng, D., Zhang, X., 2015. A modified model of solar collector/regenerator considering effect of the glazing temperature. International Journal of Refrigeration, 49, 151-159, DOI: https://doi.org/10.1016/j.ijrefrig.2014.10.004.

Rehman, N. U., Uzair, M., 2021. Hybrid ray tracing model and particle swarm optimization for the performance of an internally reflecting solar still with a booster reflector. Arabian Journal for Science and Engineering, 46, 2021-2032, DOI: 10.1007/s13369-020-04963-z.

Sutherland, I. E., Hodgman, G. W., 1974. Reentrant polygon clipping. Communications of the ACM, 17(1), 32-42, DOI: 10.1145/360767.360802.

Taler, D., Taler, J., 2017. Simple heat transfer correlations for turbulent tube flow. E3S Web of Conferences, 13(4), DOI: 10.1051/e3sconf/20171302008.

Yang, R., Wang, P. L., 1998. Experimental study for a double-glazed forced-flow solar collector/regenerator. Journal of Solar Energy Engineering, 120(4), 253-259, DOI: 10.1115/1.2888128.

Zheng, G. S., Worek, W. M., 1996. Method of heat and mass transfer enhancement in film evaporation. International Journal of Heat and Mass Transfer, 39(1), 97-108, DOI: 10.1016/S0017-9310(96)85009-5.